Developmental Cell
Article

CLASP Promotes Microtubule Rescue by Recruiting Tubulin Dimers to the Microtubule

Jawdat Al-Bassam,[1,*] Hwajin Kim,[3] Gary Brouhard,[4] Antoine van Oijen,[1,5] Stephen C. Harrison,[1,2] and Fred Chang[3,*]
[1]Department of Biological Chemistry and Molecular Pharmacology
[2]Howard Hughes Medical Institute
Harvard Medical School, Boston, MA 02115, USA
[3]Department of Microbiology and Immunology, Columbia University College of Physicians and Surgeons, New York, NY 10032, USA
[4]Department of Biology, McGill University, Montréal, QC H3A 1B1, Canada
[5]Present address: Zernike Institute for Advanced Materials, University of Groningen Nijenborgh, 9747 AG, Netherlands
*Correspondence: jawdat@crystal.harvard.edu (J.A.-B.), fc99@columbia.edu (F.C.)
DOI 10.1016/j.devcel.2010.07.016

SUMMARY

Spatial regulation of microtubule (MT) dynamics contributes to cell polarity and cell division. MT rescue, in which a MT stops shrinking and reinitiates growth, is the least understood aspect of MT dynamics. Cytoplasmic Linker Associated Proteins (CLASPs) are a conserved class of MT-associated proteins that contribute to MT stabilization and rescue in vivo. We show here that the *Schizosaccharomyces pombe* CLASP, Cls1p, is a homodimer that binds an αβ-tubulin heterodimer through conserved TOG-like domains. In vitro, CLASP increases MT rescue frequency, decreases MT catastrophe frequency, and moderately decreases MT disassembly rate. CLASP binds stably to the MT lattice, recruits tubulin, and locally promotes rescues. Mutations in the CLASP TOG domains demonstrate that tubulin binding is critical for its rescue activity. We propose a mechanism for rescue in which CLASP-tubulin dimer complexes bind along the MT lattice and reverse MT depolymerization with their bound tubulin dimer.

INTRODUCTION

Microtubules (MTs) are dynamic polymers that exhibit two transitions: catastrophe, in which an assembling MT-plus end switches to rapid disassembly, and rescue, in which a plus end ceases disassembly and begins growing again (for review, see Akhmanova and Steinmetz, 2008). In addition to intrinsic properties of tubulin polymerization, MT-associated proteins (MAPs) participate in regulating MT dynamics in vivo. The mechanisms responsible for MT rescue are perhaps the least understood aspect of MT polymerization dynamics.

Cytoplasmic linker associated proteins (CLASPs) are members of a conserved class of MAPs that stabilize specific groups of MTs in yeast, plants, and animals. CLASPs include *Saccharomyces cerevisiae* Stu1 (Yin et al., 2002), *S. pombe* Cls1p (also called Peg1), *Drosophila melangaster* MAST/Orbit (for review, see Bratman and Chang, 2008), *Arabidopsis thaliana* CLASP (Ambrose et al., 2007), and human CLASP1 and CLASP2 (Sousa et al., 2007). CLASPs have a broad range of functions in cell motility and mitosis and associate with the MT plus-ends and MT lattices (Mimori-Kiyosue et al., 2005; Kumar et al., 2009). CLASPs localize at kinetochores, the mitotic spindle midzone, centrosomes, the Golgi network, and cell cortex (for review, see Bratman and Chang, 2008; Kumar et al., 2009; Efimov et al., 2007). They contribute to the formation and maintenance of the mitotic spindle and regulate MT stability and growth at kinetochores and spindle midzone (Pereira et al., 2006; Laycock et al., 2006; Maiato et al., 2003a, 2005). In migrating fibroblasts, CLASPs are needed for a robust polarization of the MT cytoskeleton; their depletion causes an increase in the dynamics of anterior MTs and a decrease in rescue frequency (Drabek et al., 2006; Wittmann and Waterman-Storer, 2005; Mimori-Kiyosue et al., 2005). Inactivating mutations of *Drosophila* MAST/Orbit leads to defects in axonal growth cone motility (Lee et al., 2004).

CLASPs are targeted to different cellular processes through their interactions with other proteins. EB1 recruit a diverse group of +TIP proteins including some CLASPs to growing MT plus ends, by binding their Ser-X-Ile-Pro motifs (Honnappa et al., 2009; Kumar et al., 2009; Galjart et al., 2005; Mimori-Kiyosue et al., 2005). In *S. pombe*, an interaction with Ase1 (PRC1 ortholog) localizes Cls1p to regions of antiparallel MT bundling at the spindle midzone and in interphase MT bundles (Bratman and Chang, 2007). Interactions with the LL5β complex, GCC185 and CENP-E target human CLASP to the plasma membrane, Golgi network, and kinetochores, respectively (Lansbergen et al., 2006; Efimov et al., 2007; Maffini et al., 2009). CLASP has also been shown to bind to MTs directly (Wittmann and Waterman-Storer, 2005; Mimori-Kiyosue et al., 2005).

Studies of *S. pombe* CLASP, Cls1p, indicate that it promotes MT rescue events (Bratman and Chang, 2007). Cls1p is not detectable at MT plus ends but localizes to the MT lattice within MT bundles. Cls1p is essential for the frequent rescue events that maintain MTs in spindle midzone (Bratman and Chang, 2007; Grallert et al., 2006). In interphase cells, Cls1p localizes to dots near the middle of the MT bundles. Cls1p is required for all detectable rescue events, and *cls1* mutant strains exhibit no defects in other MT kinetic parameters (Bratman and Chang, 2007). Overexpression of Cls1p causes it to accumulate all along the MT lattice and greatly increases rescue frequency (Bratman

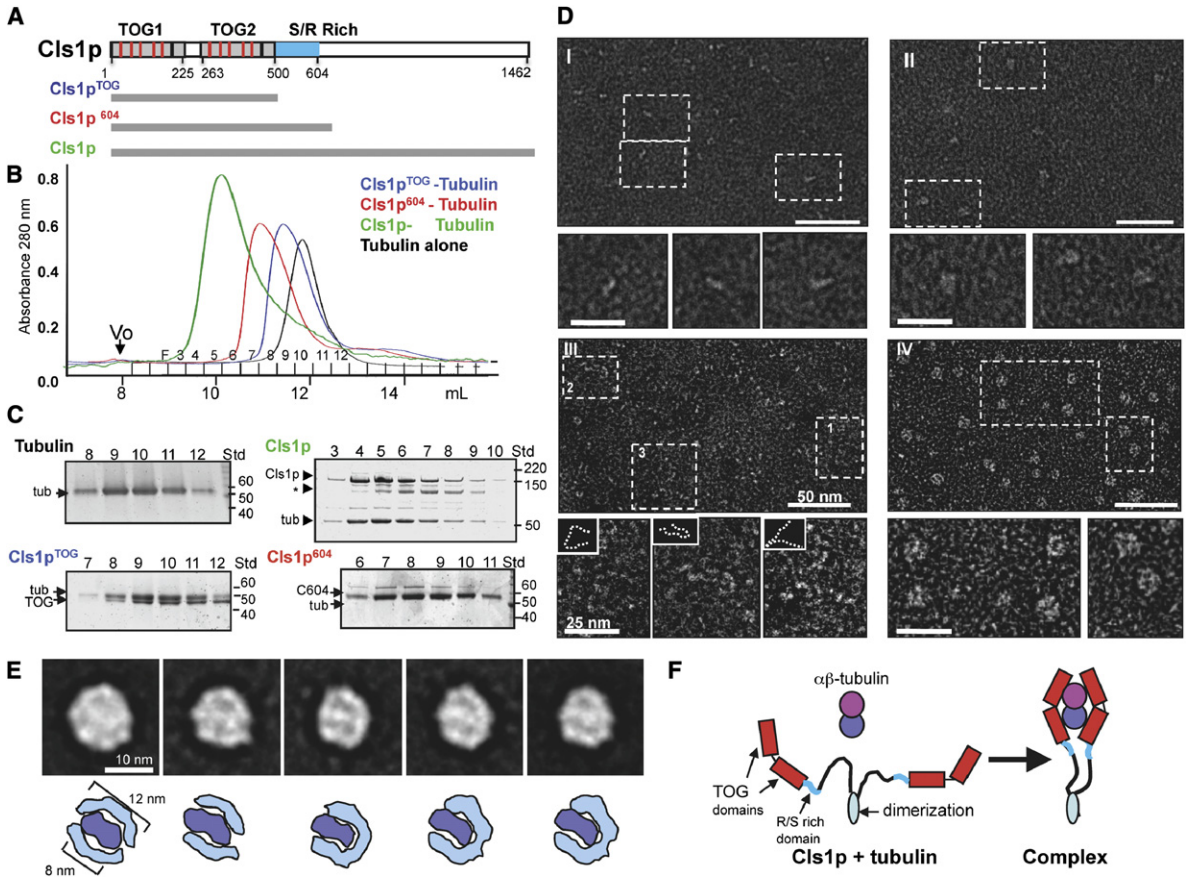

Figure 1. CLASP Wraps around a Tubulin Dimer with Two Sets of TOG Domains

(A) Domains of Cls1, as a typical CLASP protein. TOG-like and serine/arginine (S/R)-rich domains are in gray and blue, respectively. Studies with Cls1p^{TOG} (residues 1–500), Cls1p^{604} (residues 1–604), and full-length Cls1p (residues 1–1462) are described in this figure. CLASPs contain two TOG-like domains each with five, tubulin-binding, intra-HEAT repeat turns (red lines in upper panel) identified by structure-based sequence alignments with XMAP215/Dis1 TOG domains (detailed in Figures S1A and S1B).

(B and C) Size exclusion chromatography of recombinant *S. pombe* Cls1p constructs. Intensity traces of Cls1p^{TOG} (blue) and Cls1p^{604} (red) in complexes with soluble tubulin dimers indicate that Cls1p-tubulin complexes elute earlier than tubulin dimer alone (black). Cls1p-tubulin (green) elutes earlier than all other complexes, suggesting an extended conformation. SDS-PAGE of fractions from size exclusion chromatography (C); Cls1p^{TOG} and Cls1p^{604} coelute with tubulin as complexes containing one Cls1p: one tubulin. The Cls1p^{604}-tubulin complex elutes substantially earlier than Cls1p^{TOG}-tubulin, indicating a higher Stokes radius (Table S1). SDS-PAGE of fractions from Cls1p-tubulin complex peak shows that the peak saturates with a stoichiometry of two cls1p to one tubulin dimer, 2-fold higher than the Cls1p^{TOG} and Cls1p^{604} constructs. Asterisk (*) shows a very small amount of degraded inactive Cls1p. Table S1 and Figure S2 show that Cls1p is a dimer that binds a single tubulin dimer tightly, while Cls1p^{TOG} and Cls1p^{604} are monomers that dissociate quickly from tubulin.

(D) Negative stain electron microscopy of Cls1p and Cls1p^{TOG} in the presence and absence of tubulin dimer. (D,I) Cls1p^{TOG}; higher magnification images below (D,I) show that the elongated Cls1p^{TOG} molecules are ~10 nm in length. In (D,II), images of purified Cls1p^{TOG}-tubulin dimer complexes immediately after size exclusion chromatography elution. Cls1p^{TOG} appears to bind a tubulin dimer along its length. (D,III) Full-length Cls1p appears to be extended and contain flexible linkers. (D,IV) Full-length Cls1p-tubulin complexes are compact particles of uniform globular shape. Line traces of the lower magnification images in panel III are shown as broken lines as insets above each higher magnification image below (D,III).

(E) (Upper panel) Images of five representative class averages from a reference-free classification of 2700 full-length Cls1p-tubulin single particle images. The full image classification (Figure S2C) shows that Cls1p-tubulin complexes are homogenous with defined substructure. In each class average, two thin rim densities, about 12 nm in length encircle an elongated 8 nm density at the center of the particle. (Lower panel) Interpretive drawing showing the outer rim densities as two sets of TOG domains (cyan) and the central density as a single tubulin dimer (blue).

(F) Model for the CLASP conformational change accompanying the binding of a tubulin heterodimer. The C-terminal domains (900 residues) of Cls1p are flexibly linked with respect to the tubulin complex.

and Chang, 2007). Although Cls1p associates with CLIP-170 and EB1 (Grallert et al., 2006), its stabilizing effect on MTs is independent of these +TIPs and other MT-associated proteins (Bratman and Chang, 2007), suggesting that CLASP regulates MTs directly.

CLASP orthologs share a common domain organization (Figure 1A). In *S. pombe* Cls1p, conserved N-terminal sequences are critical for function, and a fragment of Cls1p containing these N-terminal domains plus the serine/arginine-rich (S/R-rich) sequences, which follow them in the polypeptide chain, are sufficient when overexpressed for MT stabilization function and to rescue viability (Bratman and Chang, 2007). Likewise, the N-terminal domains are necessary for MT stabilization in motile fibroblasts and mitotic cells (Wittmann and Waterman-Storer,

2005). It has been proposed that this N-terminal region has weak similarity to HEAT repeats characteristic of Tumor Overexpressed Gene (TOG) domains of MT polymerases, XMAP215 and its orthologs, which mediate tubulin dimer binding (Bratman and Chang, 2007; Al-Bassam et al., 2006, 2007; Slep and Vale, 2007). The C-terminal regions of CLASP have been implicated in binding the MT lattice (Wittmann and Waterman-Storer, 2005).

We describe here a mechanistic and structural analysis of *S. pombe* Cls1p. We show that the N-terminal region of Cls1p indeed contains two active Tumor Overexpressed Gene (TOG) domains that are similar to XMAP215 TOG domains. A Cls1p dimer binds a single αβ-tubulin heterodimer through two sets of TOG domains, and to the MT lattice through a serine arginine-rich domain. Despite this similarity, Cls1p behaves very differently from XMAP215, and has quite different effects on MT dynamics. In vitro, purified recombinant Cls1p is sufficient to promote MT rescue and to suppress MT catastrophe. The TOG-tubulin interaction is critical for rescue activity in vitro and in vivo. We propose that Cls1p promotes MT rescue by delivering tubulin dimers to the plus end. These studies provide a mechanistic model for MT rescue events in cells.

RESULTS

CLASP Binds a Soluble Tubulin Dimer with Two Sets of TOG Domains

Sequence alignment based upon the structures of XMAP215/Stu2 TOG domains suggests that CLASPs from various organisms contain two consecutive N-terminal TOG domains (TOG1 and TOG2), in which the amino acid residues in the predicted tubulin binding turns are similar to the corresponding residues in the XMAP215/Dis1 TOG domains (see Figure S1 available online). A region toward the C terminus of human CLASP has also been proposed to be TOG-like (Slep and Vale, 2007; Slep, 2009), but it is not conserved in other organisms and deviates substantially from TOG consensus in the length and composition of the putative tubulin-binding loops.

We tested whether the N-terminal TOG-like domains of CLASP bind tubulin. We expressed and purified full-length *S. pombe* Cls1p (residues 1–1462) and two shorter fragments: Cls1p^{TOG} (residues 1–500), containing just the two TOG domains, and Cls1p^{604} (residues 1–604), including the TOG domains and the S/R-rich region (Figure 1A). Size-exclusion chromatography showed that full-length Cls1p does indeed bind soluble tubulin dimer to form a stable complex (Figures 1B and 1C; Table S1 available online); the Cls1p^{TOG} or Cls1p^{604} fragments are sufficient to bind tubulin, but their tubulin complexes are unstable.

Size exclusion chromatography showed that full-length Cls1p has a large apparent molecular mass (Figure S2A and Table S1). By adding increasing amounts of Cls1p and determining the amount required to shift a constant amount of tubulin dimer into the complex peak, we found that the Cls1p-tubulin complex has a stoichiometry of two Cls1p molecules for each αβ-tubulin dimer (Figure S2A). Sedimentation equilibrium ultracentrifugation showed that Cls1p and Cls1p-tubulin complex have masses of 267 ± 15 kDa and 370 ± 25 kDa, respectively (Table S1 and Figure S2B). These results indicate that that Cls1p is homodimer and that the Cls1p-tubulin complex contains a Cls1p dimer bound with a single tubulin dimer.

Cls1p^{604} or Cls1p^{TOG} are monomeric, as measured by sedimentation equilibrium ultracentrifugation, suggesting that sequences C-terminal to the S/R rich domain determine dimerization (Table S1) (Grallert et al., 2006). These fragments dissociated from soluble tubulin dimers shortly after size exclusion chromatography, indicating they have lower affinity for tubulin than full-length Cls1p (Table S1). Weak binding of one set of TOG domains to tubulin dimer in a Cls1p^{TOG} monomer and strong binding of full-length Cls1p dimer are also properties of Stu2p, the *S. cerevisiae* XMAP215 ortholog (Al-Bassam et al., 2006). They suggest that dimerization enhances tubulin dimer binding.

We next studied Cls1p and shorter fragments and their tubulin complexes by electron microscopy. Images of negatively stained Cls1p^{TOG} fragment showed that the Cls1p^{TOG} domains form an extended structure, about 10 nm long and 2 nm wide. Images of Cls1p^{TOG}-tubulin complexes showed more isometric particles, about 8 nm in diameter; these may represent a 1:1 association of the Cls1p^{TOG} fragment with αβ-tubulin dimers, which are 8 nm in length (Figure 1D, panel II, data not shown). In contrast, full-length Cls1p appeared as an extended structure with two thin "tentacles," each shaped like Cls1p^{TOG} (Figure 1D, panel I). Images of purified Cls1p-tubulin complex showed uniform globular complexes, 12 nm in diameter (Figure 1D, panel II). Reference-free classification of 2700 Cls1p-tubulin particle images in SPIDER showed that these particles are extremely homogenous with relatively small differences among 45 classes (Figure 1E; full classification is shown in Figure S2C). Class averages containing the highest numbers of particles showed the Cls1p-tubulin complex to be a regular isometric particle, 12 nm in diameter, with two thin, elongated densities surrounding a ~8 nm density at the particle center (Figures 1E and S2C). One interpretation is that two sets of TOG domains (each about 12 nm in length) encircle a tubulin dimer (8 nm long) in the complex, forming a particle that is about 30–34 nm in circumference (Figure 1F; Al-Bassam et al., 2006). These EM images of the Cls1p TOG domains, full-length proteins and the tubulin-complex are all very similar to those seen with XMAP215 and Stu2p (Brouhard et al., 2008; Al-Bassam et al., 2006). Thus, at a structural level, the CLASP and XMAP215/Stu2 TOG domain have a common mode of tubulin binding.

SR-Rich Domains Contribute to High-Affinity Binding to the MT Lattice

We tested in cosedimentation experiments whether Cls1p and its fragments bind MTs. Full-length Cls1p pelleted with GMPCPP stabilized MTs, with half maximal binding at 70 nM Cls1p (Figure 2C). The binding saturated at one Cls1p monomer per approximately six polymerized tubulin dimers. This behavior is different from that of XMAP215, which exhibits only low affinity and nonsaturating MT binding (Figure S2B). Cls1p^{604} also bound MTs with high affinity, whereas Cls1p^{TOG} exhibited no significant MT binding and remained in the supernatant (Figures 3A and 2D). Cls1p^{604} binding saturated at 1 Cls1 molecule per approximately three polymerized tubulin dimers of the MT (Figure 2B). We conclude that the S/R region, which is present in Cls1p^{604} but not in Cls1p^{TOG}, mediates the interaction with the MT lattice.

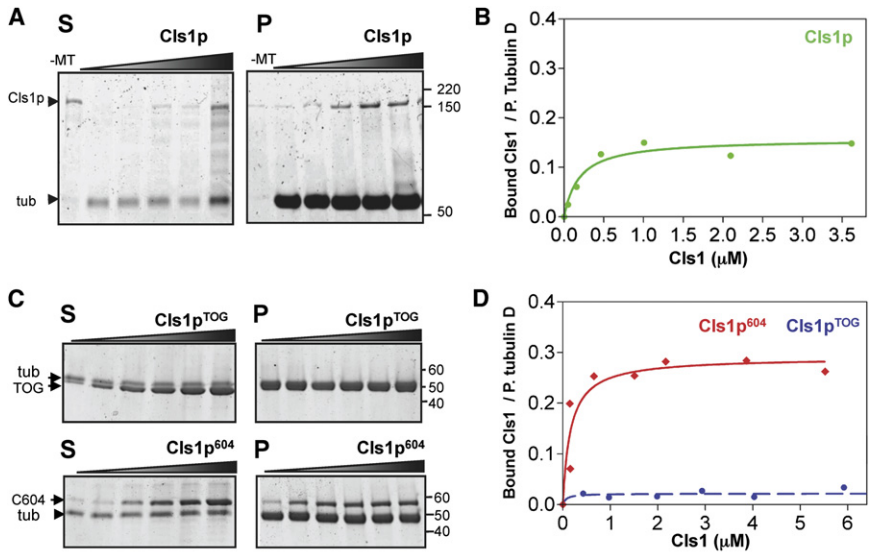

E

MT binding Isotherms	MT binding Stoichiometry *	Cls1p MT binding affinity ‡	Residual (R^2)
Cls1p	0.15 ± 0.01*	70 ± 10 nM	0.99
Cls1p^{TOG}	0.021 ± 0.004*	N/A	0.98
Cls1p^{604}	0.29 ± 0.03*	160 ± 40 nM	0.98

* MT Binding stoichiometry expressed in mole bound Cls1p monomers per mole Polymerized tubulin dimer. ‡ The concentration of Cls1p at half-maximal MT binding

Figure 2. CLASP S/R Rich Domains Bind MT Lattices with High Affinity

(A) Cls1p cosedimentation with GMPCPP-stabilized MTs. SDS-PAGE of separated pellet (P) and supernatant (S) at low concentration, Cls1p is fully MT-bound (pellet), whereas at higher concentrations excess Cls1p is unbound (supernatant). Cls1p does not sediment in the absence of MTs (-MT lanes). Tubulin dimer does not affect Cls1p binding to GMPCPP-MTs (Figure S1A). Unlike Cls1p, XMAP215 does not bind GMPCPP-MTs with high affinity (Figure S2B).

(B) Binding isotherm of Cls1p and GMPCPP-stabilized MTs determined from data shown in (A) (see Experimental Procedures).

(C) MT cosedimentation analysis of Cls1p^{TOG}, Cls1p^{604} constructs. (Lower panel) Cls1p^{604} (containing S/R-rich domain) binds and sediments with GMPCPP-MTs with high affinity, while the top panel shows that Cls1p^{TOG} does not sediment with MTs.

(D) MT binding isotherms for Cls1p^{TOG} and Cls1p^{604} determined from data shown (C).

(E) MT binding affinities and MT binding stoichiometries, in moles of Cls1p monomer per polymerized tubulin dimer, for full-length Cls1p, Cls1p^{TOG}, and Cls1p^{604}.

To determine whether TOG-domain binding of tubulin dimer affects Cls1p association with MTs, we compared MT binding in the absence and presence of 50 nM Alexa-Fluor-488-labeled tubulin dimers. The addition of soluble tubulin dimer did not influence the affinity of Cls1p for MTs (Figure S3A). These results indicate that Cls1p has two separable functions: binding to tubulin dimer and binding to the MT lattice.

CLASP Promotes MT Rescue and Suppress MT Disassembly and Catastrophe

We analyzed the effects of Cls1p on the dynamics of individual MTs by total internal reflection fluorescence (TIRF) microscopy using a modified version of methods developed for work on XMAP215 (see Experimental Procedures). Texas-red-labeled MT seeds were assembled with the nonhydrolysable GTP analog, GMPCPP (Figure 3A). Addition of a mixture of Alexa-Fluor-488-labeled and unlabeled tubulin allowed us to visualize the dynamic behavior of MTs growing from the plus ends of these stable MT seeds (Figure 3B). Dynamic MTs in vitro undergo stochastic "catastrophes," when the MT switches from assembly to disassembly, and "rescues," when assembly reinitiates. At 6 μM tubulin concentration (in the absence of XMAP215 or Cls1p), assembly is relatively slow (0.43 ± 0.03 μm/min), catastrophes are frequent (0.30 ± 0.05 catastrophes/min), and MT rescues are not observed. As Brouhard et al. (2008) previously observed, addition of 50 nM XMAP215 increased the average rate of MT assembly 10-fold and increased MT length distributions but did not affect catastrophe frequency, disassembly rate, or rescue frequency (Table S2 and Figure S4).

Addition of 40 nM Cls1p led to many rescue events (as defined by the reinitiation of assembly before disassembly has reached the seed; Figures 3C,IV and 3C,V) and a decrease the apparent frequency of catastrophes (Figure 3C,III). Some dynamic MTs assembled continuously, with no evident catastrophes in the time frame (20 min) of the experiment (Figure 3C,III), while other MTs underwent occasional catastrophe followed promptly by a rescue (Figures 3C,IV and 3C,V). To determine dose-dependent activities of Cls1p, we measured MT dynamic parameters at a series of Cls1p concentrations (Table S2 and Figure S4) (20–140 nM). As Cls1p concentration increased, the catastrophe frequency declined by 6-fold and the rescue frequency increased, reaching a plateau of 0.06 catastrophes/min and 2.15 rescues/min. The average total assembly time increased slightly with increasing the Cls1p concentration up to 13.5 min, almost 40% higher than that with 6 μM tubulin (Table S2). Thus, at 140 nM Cls1p, a single catastrophe during a 20 min period was, on average, reversed by a rescue, which occurred at least once per 30 s of disassembly (Figure 3I). The disassembly rate decreased with increasing Cls1p concentration, from 43 μm/min to 25 μm/min; the average disassembly time increased up 2-fold with increasing Cls1p concentration, due to the decrease in disassembly rate (Table S2). The assembly rate increased linearly up to 2-fold at 140 nM Cls1p. The linear increase in the assembly rate is very different from the increase observed with XMAP215, which accelerates assembly at the lower concentrations by more than 10-fold (see above) (Brouhard et al., 2008). The average dynamic MT length increased with increasing Cls1p concentration (Table S2 and Figure S4E).

At the highest Cls1p concentrations (70 and 140 nM), we observed a bimodal distribution for the dynamic MT lengths with two classes: 4.5–5.0 μm and 10–11 μm (Figure S4F and Table S2). At 140 nM Cls1p, however, many MTs in the latter group were even longer (Figure S4F).

We also tested the activity of the monomeric Cls1p^{604}, with a single set of TOG domains and an S/R rich sequence. Addition of 200 nM Cls1p^{604} produced no observable rescue and a 3-fold higher catastrophe frequency than with full-length Cls1p (Table S2 and Figure S4C). The average disassembly rate was 45 μm/min, similar to the disassembly rate for tubulin alone (Table S2 and Figure S4B). MTs were 2-fold longer (Table 2 and Figure S4E). The weakened effect of this Cls1p fragment on MT dynamics is consistent with its weakened grip on the tubulin dimer.

CLASP Recruits Tubulin Dimers to the MT Lattice

To visualize the behavior of Cls1p molecules, we expressed Cls1p with GFP fused to its C terminus. This GFP fusion is functional in vivo and can replace the endogenous Cls1p in the cell (Bratman and Chang, 2007). In vitro, the fused GFP does not affect free tubulin dimer binding and binds tubulin with a similar stoichiometry to untagged Cls1p (Table S1 and Figure S5A). Cls1p-GFP is a well-behaved dimer (300 ± 16 kDa), and Cls1p-GFP tubulin complexes (400 ± 12 kDa) contain a single tubulin dimer, just as do complexes with untagged Cls1p (Figure S5B). Furthermore, addition of GFP does not alter the effects of Cls1p on rates of MT catastrophe and rescue (see next section).

Using TIRF microscopy, we observed that Cls1p-GFP bound along MTs (Texas-red-labeled GMPCPP-MTs; Figure 4, middle panel). When added at 50 nM, the distribution of Cls1p-GFP was nonuniform and punctate; the nonuniformity decreased as binding saturated at higher concentrations (data not shown). Time-lapse images showed that the pattern of bound Cls1p-GFP puncta did not change during the course of the experiment (Figure 4A, lower panel), suggesting a stable association of Cls1p-GFP with the MT lattice.

To determine whether Cls1p molecules can bind soluble tubulin dimers while attached to MT lattices, we added untagged Cls1p and Alexa-Fluor-488-labeled tubulin dimers to MTs (Figure 4B, upper panel; see Experimental Procedures). Alexa-Fluor-488-tubulin dimers were detected along GMPCPP MTs (Figure 4B, middle panel). This binding depended on addition of Cls1p. Bulk MT cosedimentation experiments independently confirmed this finding (Figure S3A,IV). Like Cls1p, the distribution of Alexa-Fluor-488-tubulin dimers along GMPCPP-MTs was nonuniform, and there was little or no longitudinal diffusion (data not shown). The pattern of the tubulin dimers was slightly more dynamic than that of Cls1p-GFP, however, suggesting that tubulin dimers occasionally disassociated from Cls1p on the MT, with a mean residence time of 3–4 min. We further confirmed that Texas-red-labeled tubulin dimers and Cls1-GFP directly colocalized along nonlabeled GMCPP-MTs (Figure 4C). Thus, Cls1p dimers can bind tightly along MT lattices without diffusion, producing a nonuniform, punctate distribution, while retaining soluble tubulin heterodimers through TOG-domain interactions, with a slow exchange rate.

To determine the nature of Cls1p-GFP binding along lattices of GMPCPP-MTs, we tracked Cls1p-GFP puncta formed at a low Cls1p concentration (10 nM) and measured their diffusion rate. Cls1p-GFP puncta have a very low diffusion coefficient (D = 0.0015 μm^2/s) along GMPCPP-MT lattices (see Figure 4D), significantly (135-fold) lower than the diffusion coefficient for XMAP215 (D = 0.2 μm^2/s; Brouhard et al., 2008). This difference is consistent with the difference in their MT affinities derived from bulk MT cosedimentation (Figure 2D and S3B). We conclude that the Cls1p binds the MT lattice tightly, while XMAP215 has weaker, largely electrostatic interactions that allow it to diffuse along the MT.

We asked whether the nonuniform distribution of Cls1p indicates that Cls1p molecules cluster together on the MT lattice through interactions among Cls1p molecules, or could simply reflect random binding along the MTs. We performed a computational simulation of Cls1p binding, using a "model convolution" approach (Gardner and Odde, 2010). The simulation generated artificial images of Cls1p-GFP on MTs, which were compared with experimental distributions (Figure 4E). Under conditions of a random distribution, Cls1p molecules produced images with nonuniform patches reminiscent of fluorescence speckling of Cls1p-GFP along MT lattices (Figure 4F, panel 1). A simulation that explicitly introduced weak oligomerization or clustering (see Experimental Procedures) also produced images consistent with our data (Figure 4F, panel 2), but increasing the propensity of Cls1p to oligomerize caused the artificial Cls1p images to diverge from the experimental data (Figure 4F, panels 3 and 4). Comparing these artificial images with experimental data, we conclude that the nonuniform distribution of Cls1p-GFP puncta seen experimentally probably arises from the Poisson statistics that underlie random high affinity binding along the MT lattice, but we cannot rule out a limited degree of self-association and clustering among Cls1p molecules.

MT Rescues Occur at Sites of a High Local Concentration of CLASP Molecules

We devised a two-color TIRF experiment to determine the behavior of Cls1p on dynamic MTs, and to visualize Cls1p-mediated MT rescue events directly. The dynamic portion of the MT and the MT seeds were both labeled with Texas red, but the difference in fluorescence intensities allowed us to identify dynamic transitions unambiguously (Figures 5B, 5S, and 5D denote seed and dynamic MTs, respectively). We used a 70 nM mixture of Cls1p-GFP (10 nM) with untagged-Cls1p (60 nM) to decrease background; activities of this mixture were similar to those of 70 nM Cls1p (Table S2 and Figure S4, 2C-TIRF panels).

We noted first that Cls1p-GFP bound more densely into nonuniform puncta along the MT seeds than along the dynamic MTs, even when the latter remained polymerized throughout the experiment (Figures 5C, 5D, and S6A). As the principal difference between the two MT forms is the nucleotide state of the polymerized tubulin (mostly GTP-like in the MT seed, and mostly GDP-like in the dynamic MT), it is possible that Cls1p has some preference for polymerized GTP tubulin in the MT lattice.

On the dynamic MTs, we observed that Cls1p-GFP bound with a combination of diffuse and punctate distributions along the lattice and near MT plus ends, but with a lower density than along the MT seeds (Figure 5C). The sites of MT rescues were anticipated by Cls1p-GFP puncta, which are the sites of high local

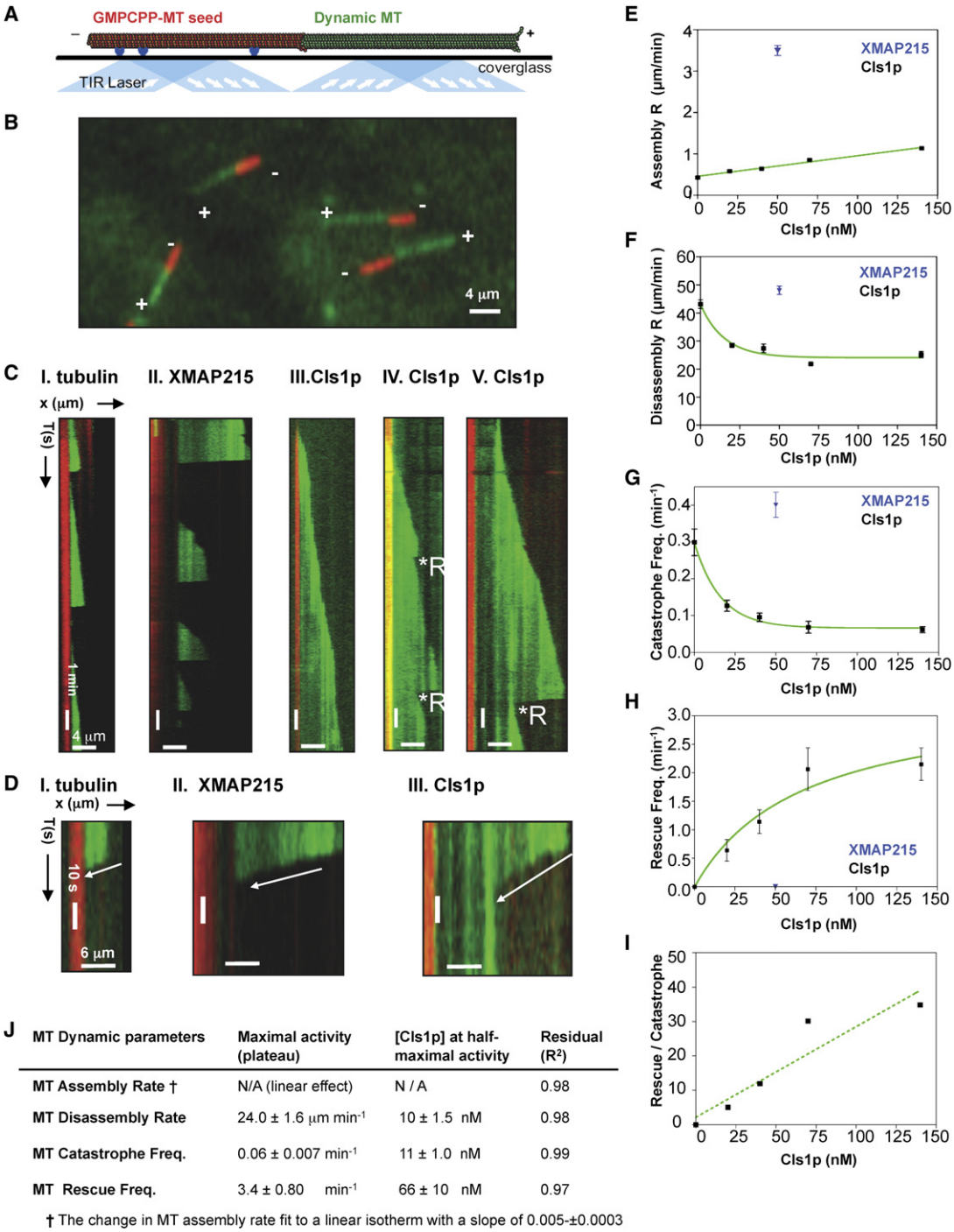

J

MT Dynamic parameters	Maximal activity (plateau)	[Cls1p] at half-maximal activity	Residual (R^2)
MT Assembly Rate †	N/A (linear effect)	N / A	0.98
MT Disassembly Rate	24.0 ± 1.6 μm min^{-1}	10 ± 1.5 nM	0.98
MT Catastrophe Freq.	0.06 ± 0.007 min^{-1}	11 ± 1.0 nM	0.99
MT Rescue Freq.	3.4 ± 0.80 min^{-1}	66 ± 10 nM	0.97

† The change in MT assembly rate fit to a linear isotherm with a slope of 0.005-±0.0003

Figure 3. Effect of CLASP on MT Dynamics Parameters

(A) Scheme for total internal refection fluorescence (TIRF) microscopy used to study MT dynamics. Surface-attached antibiotin antibodies (blue) bind biotin-labeled GMPCPP-stabilized MT seeds (red). The seeds near the surface nucleate Alexa-Fluor-488-labeled (green) dynamic MTs from 6 μM soluble tubulin dimers in the presence of GTP. TIRF illumination by 568 and 488 nm lasers. Image adapted from Brouhard et al. (2008) with permission from Elsevier.

(B) TIRF image of assembling MTs. Seeds (red) initiate assembly of dynamic MTs (green) at plus ends (+) only.

(C) Kymographs of assembly and disassembly of single dynamic MTs. (C,I) Six micromolars tubulin: dynamic MTs show slow assembly, rapid disassembly, and frequent catastrophes. (C,II) Fifty nanomolars XMAP215 + 6 μM tubulin: dynamic MTs show rapid MT assembly and frequent catastrophes. (C,III–C,V) Forty nanomolars Cls1p + 6 μM tubulin. (C,III) shows a relatively slow assembly MT rate and no catastrophes. (C,IV) shows a dynamic MT assembling slowly with two catastrophes, each followed by a rescue (R*). (C,V) shows a dynamic MT assembling slowly and a catastrophe that leads to extended disassembly, which is followed by a rescue.

(D) Closeup kymographs in (C) shows MT disassembly at higher time resolution.

concentration on the MT lattice (Figures 5D and S6A,I–S6A,III). Average intensity profiles showed that the site of rescue coincided with a peak in the Cls1p-GFP fluorescence to within 1 pixel (270 nm) (Figure 5E, lower panel; $p \leq 0.01$; Figure S6B,II). The average Cls1p-GFP intensity at the site of MT rescue was 3-fold higher than at sites that did not initiate rescue events. All MT rescues observed occurred at Cls1p puncta, and we did not observe rescues events at other sites. Thus, these results suggest that rescue requires a minimum local concentration of Cls1p along the MT lattice.

We did not observe Cls1p tracking with the growing MT plus end (Figures 5C, S6A,III, and S6,IV). The presence of Cls1p-GFP puncta near growing plus ends may, however, explain the decrease in MT catastrophe. (Figures 5C and S6A,IV). Catastrophes occurred with normal frequency at MT plus ends that did not accumulate Cls1-GFP puncta (Figure S6C). Rescue events occurring very near the position of catastrophe at plus ends cannot be spatially resolved by our imaging system (about 270 nm per pixel, equivalent to 34 tubulin dimers along a protofilament); such local rescues will appear as a decrease in the occurrence of MT catastrophes.

TOG-Tubulin Interaction Is Required for CLASP Function

To test the function of tubulin binding, we generated mutations to eliminate CLASP tubulin binding without disrupting its structure. The alignment of TOG domains allows us to predict the tubulin-binding surface of CLASP (Figure S1B) (Al-Bassam et al., 2007). We mutated to alanine-conserved residues in two of the intra-HEAT repeat turns (W293A in T1 and K379A and K380A in T3: Figure 6A). Multiple assays showed that this TOG domain mutant, designated Cls1p^{T1T3}, is deficient specifically in tubulin dimer binding. Its affinity for tubulin was too low for coelution in size-exclusion chromatography (Figures 6B and S7A). MT co-sedimentation experiments showed that the Cls1p^{T1T3} bound MT lattices to the same extent as wt Cls1p, and the binding isotherms suggested a similar affinity and stoichiometry (Figure S7B). TIRF experiments showed that Cls1p^{T1T3} did not recruit AlexaF-488-labeled tubulin dimer to the lattices of GMPCPP-MTs (Figures S7B and S4C).

We then examined the effect of these TOG mutations on MT dynamics in vitro. Addition of 200 nM Cls1p^{T1T3} had no effect on the frequencies of rescue or catastrophe (Figures 6B and S7B, and Table S2). In contrast, 200 nM Cls1p^{T1T3} still had effects on MT assembly and disassembly (Table S2). A Cls1p^{T1T3}-GFP fusion protein also bound nonuniformly along GMPCPP-MTs and formed puncta that were indistinguishable from those seen with Cls1p-GFP (Figure 6E). MT lattice binding and tubulin dimer binding are thus separable activities of Cls1p. These data suggest that regulation of rescue and catastrophe require tubulin dimer binding by the TOG domains, while the effects on MT disassembly and assembly are TOG-domain independent and thus may be caused by MT lattice binding activity.

We also examined the effects of the tubulin-binding mutations in vivo, by expressing these mutant proteins in *S. pombe* cells. We analyzed their localization and MT stabilizing activity using methods described previously (Table S3) (Bratman and Chang, 2007). Cls1 TOG-domain mutants (Cls1^{T1}, Cls1^{T3}, and Cls1^{T1T3}) localized normally to regions of overlap within MT bundles (Figure 6E). We determined if the TOG mutants could rescue the viability of *cls1* null cells using a spore viability assay. Wild-type Cls1-expressing plasmids displayed nearly full rescue of Cls1 function, while the vector control and each of the *cls1* TOG mutant genes showed little significant rescue (Figure 6F). To determine if TOG function is needed for MT stabilization, we induced high expression of the *cls1* mutant genes. Overexpression of mCherry-Cls1 stabilized MT bundles and bound along the MT lattices, so that they were resistant to the MT disrupting drug, methyl-benzidazole-carbamate (MBC; Bratman and Chang, 2007). In contrast, in each of the strains overexpressing the *cls1 TOG* mutants or in the vector control, MT bundles were not stabilized and shrank to single perinuclear dots (Figures 6G and 6H). A Cls1^{T5} mutant (T5 mutation: R465A) showed similar but less severe defects (Table S2). Thus, binding of Cls1p to tubulin dimer is essential for its function and for MT stabilization activity both in vitro and in vivo.

DISCUSSION

The experiments described here show that *S. pombe* CLASP, Cls1p, promotes MT rescue and suppresses catastrophe by recruiting tubulin dimer to the MT lattice. Consistent with previous studies indicating that the Cls1p is required for MT rescue in vivo (Bratman and Chang, 2007), we show that purified Cls1p alone is sufficient to mediate these activities without other proteins in vitro. Cls1p is a homodimer that captures a soluble αβ-tubulin heterodimer, encircling the tubulin with its two sets of tandem TOG domains; it also binds tightly to the MT lattice (Figure 7). The binding of tubulin dimer is required for Cls1p to regulate rescue and catastrophe, but is not required for its effects on MT polymerization and depolymerization. These findings suggest the following model for rescue (Figure 7).

(E) Effect of Cls1p concentration on MT assembly rate. Cls1p (black) accelerates MT assembly slightly, while 50 nM XMAP215 (blue) increases the assembly rate by 10-fold (Table S2; Brouhard et al., 2008). Each point (Table S2) represents the mean of Gaussian distribution fit to a large number of assembly events measured for each Cls1p concentration (distributions are shown in Figure S4A).

(F) Effect of Cls1p concentration on MT disassembly rates. Each point (Table 1) represents the mean of Gaussian distribution fits to a large number of events at different Cls1p concentrations (distributions are shown in Figure S4B).

(G) Effect of Cls1p concentration on MT catastrophe frequency (Table S2). Each point (Table S2) represents the mean from a Gaussian distribution to a large number of catastrophe frequencies measured for each Cls1p concentration (distributions are shown in Figure S4C).

(H) Effect of Cls1p concentration on the MT rescue frequency. Each point (Table S2) is the mean rescue frequency measured for each Cls1p concentration shown in Figure S4D.

(I) Effect of Cls1p concentrations on the ratio of MT rescue to MT catastrophe. At 140 nM Cls1p, on average every MT catastrophe (one event per 15.6 min of MT assembly) was reversed by a rescue (one event per 45 s of MT disassembly).

(J) Table showing fitted Cls1p concentration and maximal effects summarizing data from (E)–(I).

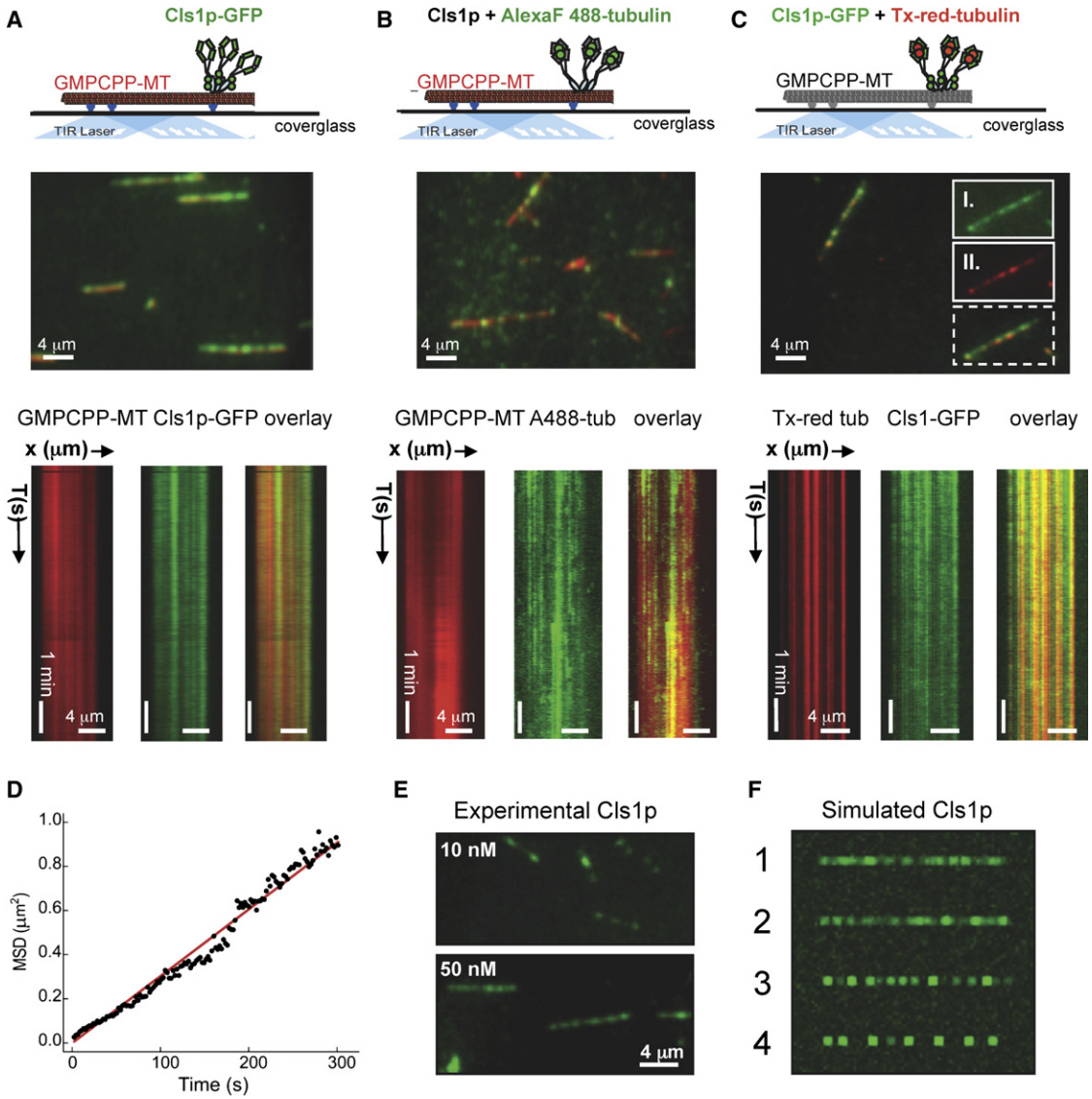

Figure 4. Cls1p-GFP Molecules Bind Nonuniformly along GMPCPP-Stabilized MTs and Recruit Soluble Tubulin Dimers

(A) (Top) TIRF experiment scheme to detect Cls1p-GFP binding to Texas red GMPCPP MTs (red). (Middle) TIRF image of 50 nM Cls1p-GFP (green) binding nonuniformly along GMPCPP MTs (red). (Bottom) Kymographs of Cls1p-GFP (green, left) on GMPCPP-MT (red, middle) in isolated channels and overlaid (right). Nonuniform patches of densely bound Cls1p-GFP remain stationary along GMPCPP MTs.

(B) (Top) TIRF experiment scheme to detect untagged Cls1p molecules (gray) recruiting Alexa-Fluor-488-labeled tubulin (green) while bound to GMPCPP MTs (red). (Middle) TIRF image of Alexa-Fluor-488-labeled tubulin dimers (green) recruited to the GMPCPP MTs (red) by bound untagged-Cls1p. (Bottom) Kymographs of Alexa-Fluor-488-labeled tubulin dimers (green, left) recruited by untagged Cls1p along GMPCPP-MTs (red, middle) in isolated channels and overlaid (right).

(C) (Top) Schematic of TIRF experiment to simultaneously detect recruitment of Cls1p-GFP (green) and Texas red tubulin (red) along nonlabeled GMPCPP MTs (gray). (Middle) TIRF image of 50 nM Cls1p-GFP (green) and 50 nM Texas red tubulin (red) binding nonuniformly along GMPCPP MTs (red). (Inset) II and I show raw images of Cls1-GFP and Texas red tubulin bound along GMPCPP MTs in the isolated channels above their overlaid image (broken lines). (Bottom) Kymographs of GMPCPP-MT (red) in isolated channels and overlaid. Nonuniform patches of densely bound Cls1p-GFP remain stationary along GMPCPP MTs. Images in top panels were adapted from Brouhard et al. (2008) with permission from Elsevier.

(D) Tracking of Cls1p puncta along dynamic MTs to determine the average diffusion coefficient (see Supplemental Experimental Procedures).

(E) Experimental images of 10 nM (top) and 50 nM (bottom) of Cls1p-GFP puncta bound along GMPCPP-MTs.

(F) Simulation of Cls1p-GFP binding along linear MT lattices comparing different degrees of self-association. (F1) A random association with MT lattice without diffusion. (F2) Weak self-association among molecules while binding to the MT lattice binding. (F3) Moderate self-association among Cls1p-GFP molecules. (F4) A high degree of self-association. Note that the degree of speckling and sharpness of puncta in experimental Cls1p-GFP images is similar to simulations in either (F1) or (F2), and different from simulations in (F3) and (F4).

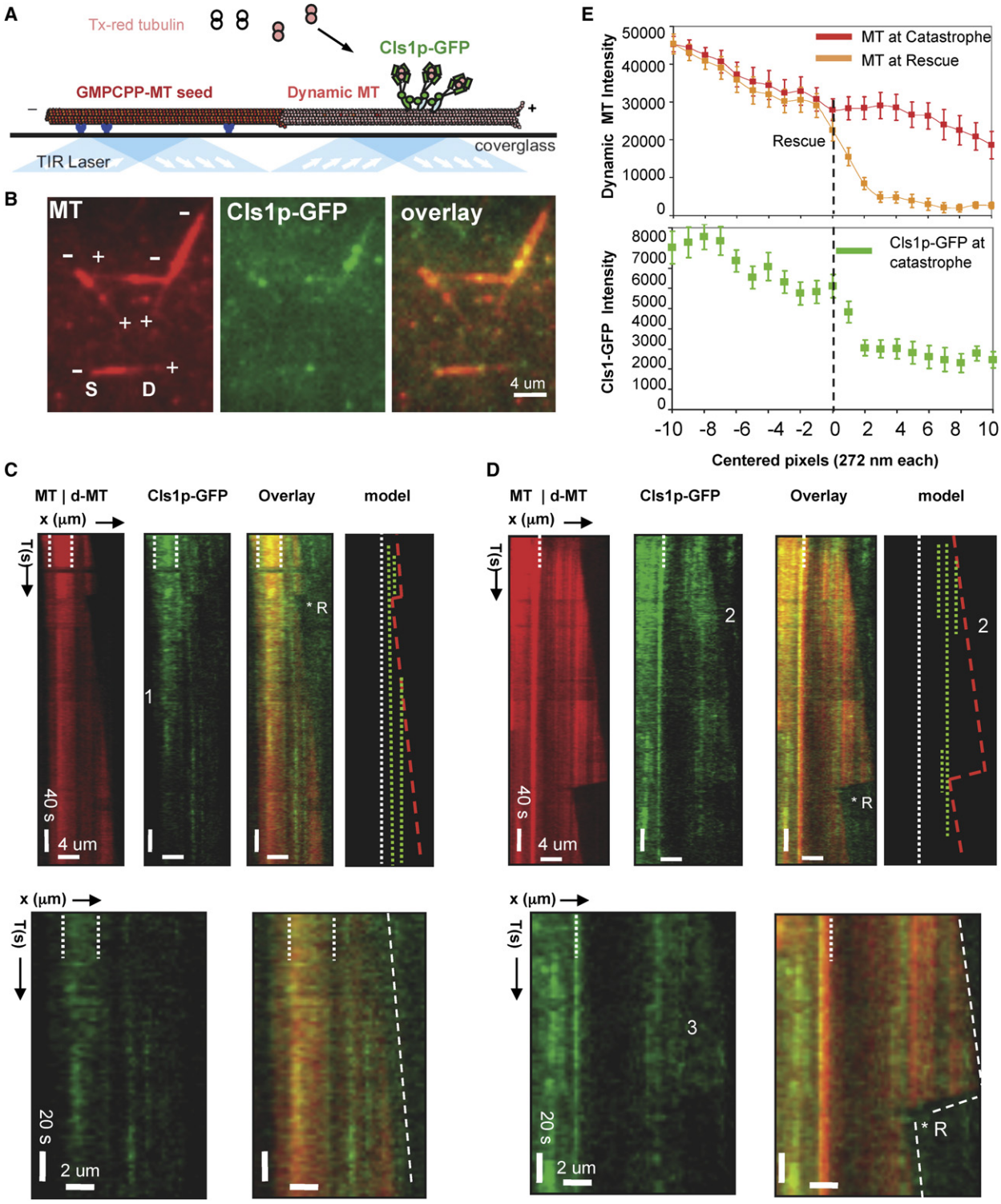

Figure 5. Sites of High CLASP Concentration Locally Anticipate Sites of MT Rescues

(A) Schematic of TIRF microscopy assay used for imaging MT dynamics and for simultaneous imaging of dynamic MTs and Cls1p-GFP localization. Anti-biotin antibodies (blue) capture biotin- and Texas red-labeled GMPCPP polymerized MT seeds (red) near the silanized glass surface. Densely labeled Texas red MT seeds nucleate dynamic MT assembly from 6 μM tubulin dimers, less densely labeled with Texas red, in the presence of GTP and Cls1p-GFP (see Experimental Procedures). Image adapted from Brouhard et al. (2008) with permission from Elsevier.

(B) Raw TIRF image of dynamic MTs and Cls1p-GFP. (Left) Dynamic MTs growing at plus ends of MT seeds. Note high fluorescence intensity of the MT seed compared with the dynamic MT. (Middle) Cls1p-GFP nonuniformly bound along dynamic MTs (middle). Cls1p-GFP accumulates more densely along the seed. (Right) Overlay of both images.

A group of Cls1p molecules clutching tubulin dimers bind on the MT lattice and await a MT depolymerization event. When a plus end shrinks to this site, these Cls1p-tubulin complexes halt depolymerization and restart growth (Figure 7). In vitro studies with pure tubulin show that rescue depends on tubulin concentration; rescues are very rare at physiological concentrations (6 μM tubulin dimer) but are more frequent at much higher concentrations (Walker et al., 1988). Thus, Cls1p could promote rescue by increasing the local tubulin dimer concentration. We envision two ways in which Cls1p could promote MT rescue (Figure 7). In one model, Cls1 molecules deliver a GTP tubulin dimer into MT plus ends to restart MT assembly. The tubulin is released and incorporated into the MT. In this model, Cls1p acts like a polymerase to promote growth. In another (not mutually exclusive) model, local clusters of Cls1p-tubulin halt protofilament disassembly by transiently stabilizing the MT plus end, presenting the bound tubulin, without necessarily releasing it onto the MT plus end. Cls1p may suppress catastrophe by a related mechanism, promoting local rescue events so close to the plus end that the disassembly phase remains undetected.

The combined in vitro and in vivo evidence makes CLASP a compelling candidate for a rescue factor. Our data show that CLASP promotes rescues at essentially physiological tubulin concentrations. In *S. pombe*, genetic studies show that Cls1p is responsible for all measurable rescue events in these cells and does not affect any other MT parameters (Bratman and Chang, 2007). Loss of CLASP in motile fibroblasts leads to a decrease of MT rescue frequency (Mimori-Kiyosue et al., 2005). Although activities of other CLASPs have not yet been examined in vitro, we propose that CLASPs have a general function in promoting MT rescue, consistent with their various biological roles. Near MT minus ends, such as at the centrosome and sites of MT nucleation at the Golgi, CLASP may wait on the MT lattice and prevent complete depolymerization, stabilizing a MT stub that is competent to grow again (Efimov et al., 2007; Bratman and Chang, 2007). At the kinetochore and at the leading edge of migrating cells, CLASP is needed for sustained MT assembly and suppression of catastrophes (Maiato et al., 2003b; Mimori-Kiyosue et al., 2005). We suggest that if CLASP is targeted to the MT plus end, it may suppress catastrophe by promoting local rescue events at plus ends so that MT disassembly is not detected.

Our work shows that CLASP is structurally related to XMAP215—another TOG-domain protein. The two sets of TOG domains in a CLASP dimer wrap around tubulin just as do the two sets of tandem TOG domains in a Stu2p dimer or those within an XMAP215 monomer (Al-Bassam et al., 2006; Brouhard et al., 2008). These proteins contact tubulin dimer through a conserved surface located in the turns between successive helices of a HEAT repeat (Al-Bassam et al., 2007; Slep and Vale, 2007). TOG domains bind free tubulin dimers and not tubulins within a MT, presumably because sites of interaction on the tubulin are occluded when the tubulin is incorporated into the lattice.

Despite their structural similarity, CLASPs and XMAP215/Dis1 proteins have quite different effects on MT dynamics. One evident difference between these proteins is how they interact with the MT lattice. XMAP215 proteins diffuse along the MT lattice and bind selectively at MT plus ends, where they accelerate both assembly and disassembly (Brouhard et al., 2008). In contrast, we detect no accumulation of Cls1p at MT plus ends either in vitro or in vivo. Instead, Cls1p molecules bind with high affinity to the MT lattice and exhibit little movement. It will be interesting to see whether other differences between the two proteins, for instance, within the TOG domain, also contribute to their differences in activity.

Several other MAPs including MAP4, MAP2, EB1, and kinesin-8 have also been shown increase MT rescue frequencies in vitro (Pryer et al., 1992; Ookata et al., 1995; Ichihara et al., 2001; Gupta et al., 2006; Katsuki et al., 2009), but in general, the in vivo significance of their rescue activities are not yet clear. Conventional MAPs, like MAP2, may promote rescue by binding and stabilizing the MT lattice (Ichihara et al., 2001), while the kinesin-8 Kif18A binds tightly to the MT plus end upon reaching the end of its motile cycle and thereby decreases MT dynamic transitions (Du et al., 2010). Our work shows that Cls1p promotes MT rescue by a mechanism distinct from those of other factors. Some recent work suggests that many MT rescue events in mammalian cultured cells occur at sites on the MT lattice that also stain with an antibody specific for the GTP form of tubulin (Dimitrov et al., 2008). It will be important to test if MAPs such as CLASP

(C) Cls1p-GFP binding along assembling dynamic MTs. (Left) Kymograph of dynamic MT (dMT) growing from a more densely labeled GMPCPP-MT seed (delimited by white broken lines). A single catastrophe occurred and was reversed by a rescue (*R). MT assembly then continued without further catastrophes. (Second from left) Cls1p-GFP molecules bind more densely along the GMPCPP MT seed than along growing MT. Photobleaching decreased Cls1p-GFP fluorescence at the position marked by the numeral 1. Sites occupied at high Cls1p-GFP concentration remain at fixed positions without diffusion. (Third from left) Sites of Cls1p-GFP binding along a growing MT. (Right) Model kymograph showing the positions of high local concentration of Cls1p-GFP (broken green lines) along dynamic MTs (boundaries in red lines). Higher magnification kymographs show Cls1p-GFP molecules bound along an assembling MT. Note the absence of MT plus-end tracking. An additional example is shown in Figure S6A,IV.

(D) Sites of high concentration of Cls1p-GFP molecules correlate with sites of MT rescue on a dynamic MT. (Left) Kymograph of dynamic MT (dMT) assembling from an intensely labeled GMPCPP-MT seed (MT, white broken lines). A catastrophe was followed by MT disassembly and a rescue (R*). (Second panel from left) Cls1p-GFP (green) binds nonuniformly and without diffusion along the dynamic MT. Note that three Cls1p-GFP bands form, but two dissociate early during assembly (marked by the numeral 2). (Third panel from left) Sites of MT rescue correlate with positions of high Cls1p-GFP density (green) on a dynamic MT (red). (Right) Model kymograph showing the position of Cls1p-GFP dense bands (broken green) compared with the dynamic MT boundary (red) growing from the GMPCPP MT seed (broken white line). Higher magnification images show correlation of Cls1p "bands" with MT rescue. Additional examples are shown in Figures S6A,I–S6A,III. Note the loss in the diffuse Cls1p-GFP fluorescence (marked by numeral 3) reproduces the MT disassembly rate. Figure S6C shows MT rescues were not observed in the absence of sites of high Cls1p-GFP concentration along dynamic MTs.

(E) Correlation of local Cls1p-GFP concentration on the MT with MT rescue. Average fluorescence intensity profile (see Experimental Procedures) of a dynamic MT before catastrophe (red profile), dynamic MT at rescue (orange profile), and Cls1p-GFP along dynamic MT before catastrophe (green profile) for 20 different rescue events (more details in Figure S6B). Note that the Cls1p-GFP intensity peaks within 1 pixel (272 nm) of the site of rescue and the increase is 3-fold higher at that site than any pixel prior. The raw intensity profiles for Cls1p-GFP with MT rescue and statistical significance of Cls1-GFP intensity increase are shown in Figure S6B.

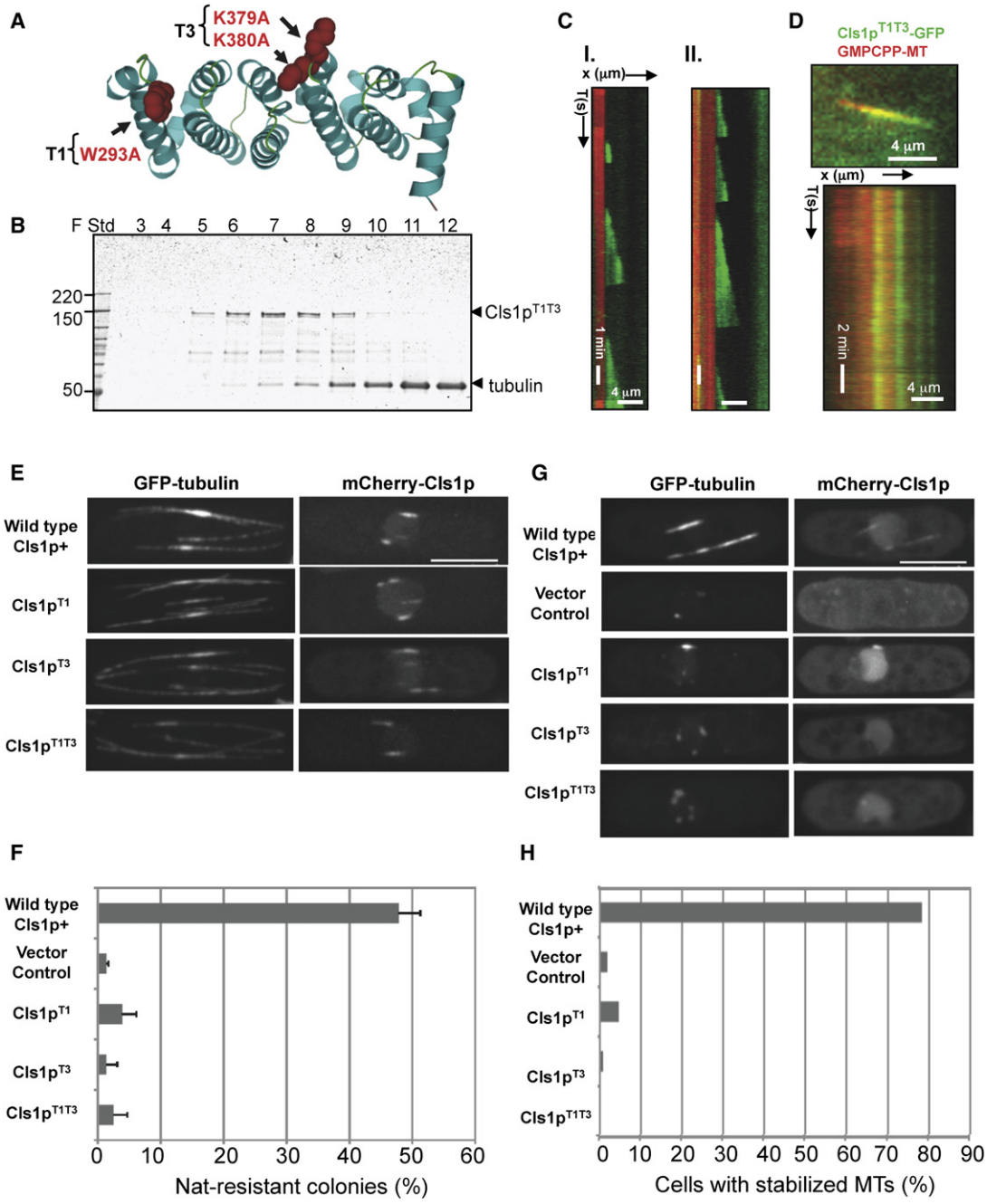

Figure 6. Defects of Cls1p Mutants with Inactivated TOG-Tubulin Interface

(A) Ribbon model of a TOG domain (PDB ID 2OF3) (Al-Bassam et al., 2007) showing W293 and K379/K380 (red space filling) in the intra-HEAT turns (T1 and T3) mutated in Cls1p^{T1T3} to disrupt tubulin dimer binding.

(B) SDS-PAGE of size exclusion chromatography fractions of Cls1p^{T1T3} with tubulin dimer, as in the experiment with Cls1p in Figure 1A. The Cls1p^{T1T3} mutant does not co elute with tubulin dimer (tub); absorbance profile is shown in Figure S7A.

(C) Kymographs of dynamic MTs assembled in the presence of 200 nM recombinant Cls1p^{T1T3} as described in Figure 3B; note the frequent catastrophes and loss of rescues. Dynamic MT parameters (Table S2), determined based on distributions, are shown in Figure S6D.

(D) Cls1p ^{T1T3}-GFP binding along GMPCPP MTs. (Top) Raw image of Cls1^{T1T3}-GFP binding nonuniformly along Texas red GMPCPP MT (red) similar to Cls1p-GFP described in Figure 4E. (Bottom) Kymograph of the Cls1p^{T1T3}-GFP (green) on GMPCPP-MT (red), showing that Cls1^{T1T3}-GFP distribution remained stationary throughout the experiment. Bulk MT cosedimentation analysis shows that Cls1^{T1T3} binds MT with an affinity similar to wt Cls1p (Figure S7B).

(E) Localization of cls1p mutant proteins in vivo. Full-length Cls1p^{T1}, Cls1p^{T3}, and Cls1p^{T1T3} were expressed as mCherry fusion proteins driven by the thiamine-repressible *nmt1** promoter in *S. pombe* cells expressing GFP-tubulin. Cells were grown in thiamine for relatively low levels of expression. Note that the localization of cls1p to regions of MT overlaps on MT bundles is not perturbed in the *cls1* TOG mutants. Maximum projection confocal images of representative cells are shown.

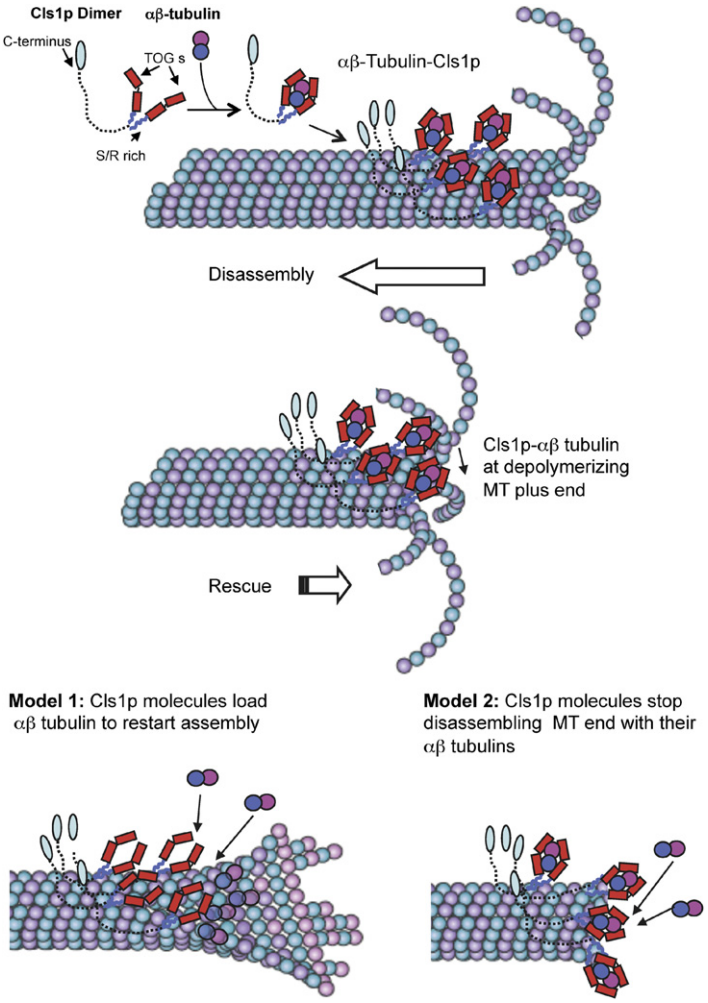

Figure 7. Mechanism of CLASP in Promoting MT Rescues

The *S. pombe* CLASP, Cls1p, is a dimer that binds a single αβ-tubulin dimer through two sets of TOG domains and binds to the MT lattice through two S/R rich domains. The C-terminal domain, shown extended, may bind other molecules. Cls1p dimers loaded with αβ-tubulin dimer bind nonuniformly along the MT lattice. When the disassembling end reaches a position of high local Cls1p density, Cls1p promotes rescue by halting disassembly and stimulating regrowth. Two models may explain Cls1p activity: model 1 shows Cls1p molecules loading their bound tubulin to MT plus end to restart assembly (left). Model 2 shows Cls1p molecules using their bound tubulin to halt protofilament and to pause MT plus end disassembly. Dynamic MT Images were adapted by permission from Macmillan Publishers Ltd: Nature Reviews Molecular Cell Biology, Akhmanova and Steinmetz (2008).

are located at these sites. We observed in our in vitro experiments that CLASP binds more readily to a GMPCPP-MT seeds than it does to the dynamic parts of the MT, suggesting that CLASP recognizes structural features of the MT lattice that reflect the nucleotide state of the polymerized tubulin. It is also possible that the GTP-tubulins associated with the MT lattice in vivo are actually GTP-tubulin dimers bound to the lattice by CLASP.

EXPERIMENTAL PROCEDURES

S. pombe Cls1p Constructs, Protein Expression, and Purification

cDNA encoding full-length *S. pombe* Cls1p, Cls1p^{T1T3} (residues 1–1462 with or without C-terminal GFP), Cls1p^{TOG} (residues 1–500), and Cls1p^{604} (residues 1–604) was cloned into a modified baculovirus expression vector. Proteins were expressed in Hi5 insect cells and purified using standard approaches, as described in detail in the Supplemental Experimental Procedures.

Biophysical Analyses of Cls1p Constructs and Their Complexes with Tubulin Dimer

Tubulin dimers were purified from bovine brains using the standard approaches (Mitchison and Kirschner, 1984). For size exclusion chromatography (SEC), Cls1p constructs were allowed to form complexes with various amounts of tubulin dimer for 5 min and were loaded onto a 10/5 Superdex 200 column pre-equilibrated at 4°C with 25 mM HEPES, 80 mM KCl, and 1 mM EGTA [pH 7.0], and eluted in 0.5 ml fractions, which were evaluated by SDS-PAGE. Apparent and measured molecular masses for Cls1p and constructs and tubulin complexes were determined by size-exclusion column and by sedimentation equilibrium analytical ultracentrifugation, respectively, as described in the Supplemental Experimental Procedures.

MT Cosedimentation

Tubulin at 1.8 mg/ml was polymerized into MTs in the presence GMPCPP for 2 hr. Various Cls1p constructs and XMAP215 were added in increasing amounts to a constant concentration (8.1 μM) of GMPCPP-stabilized MTs and cosedimented by ultracentrifugation. The contents of Cls1p and its constructs in the supernatants and pellet were determined by SDS-PAGE. Gels were scanned and quantified by densitometry of the Cls1p-protein bands. Binding curves and dissociation constants for Cls1p and other constructs were fit using Prizm software. We detect Alexa-Fluor-488 fluorescence at 488 nm in SDS-PAGE using a Typhoon imager.

Electron Microscopy of Cls1p-Tubulin Complexes

Early size exclusion chromatography fractions for Cls1p and Cls1p^{TOG} alone or in complex with tubulin dimer were diluted to 0.1 mg/ml and incubated for 2 min on glow discharged continuous carbon support on 400 copper mesh grids. Grids were washed quickly with gel filtration buffer and then stained with 0.5% uranyl formate and dried. Samples were imaged at

(F) Ability of the cls1 TOG mutant proteins to rescue viability of *cls1* null cells. Diploid *cls1*$^{+}$/*cls1Δ* cells carrying wild-type or mutant *cls1* plasmids were sporulated; resultant spores with plasmids were assayed for viability by measuring percentage of viable haploid Nat-resistant colonies carrying the *cls1Δ* allele (see Experimental Procedures). Full rescue of viability in *cls1Δ* is predicted to be 50% in this assay. Note that Cls1p ^{T1}, Cls1p^{T3}, and Cls1p^{T1T3} mutants are defective in rescuing the cls1p function in haploid cells, similar to vector control (detailed in Table S3).

(G and H) Cls1-TOG mutants are defective in MT stabilization activity. (G) Cells carrying mCherry Cls1p^{T1}, Cls1p^{T3}, and Cls1p^{T1T3} were induced for higher expression by growing in media lacking thiamine in wild-type cells expressing GFP-tubulin, and then assayed for stabilization by treatment with MT destabilizing drug, methyl-benzidazole-carbamate (MBC). Maximum projections of confocal images of representative cells are shown. Note that MT bundles are stabilized in cells overexpressing wild-type mCherry-Cls1p, which binds along the MT lattice, whereas MTs in cells overexpressing the Cls1p^{T1}, Cls1p^{T3}, Cls1p^{T1T3}, or vector controls are not stabilized and shrink to perinuclear dots. Scale bar, 5 μm. (H) Percentage of cells with stabilized cytoplasmic MTs 10 min after MBC treatment. MTs were with MBC. We considered a MT bundle as stabilized if it was ≥2 μm in length (detailed in Table S3).

52,000× magnification using a Techni-12 electron microscope (Philips) operated at 120 kV using a low dose protocol. EM images were recorded on a 2K × 2K Gatan CDD (model 894) using Digital Micrograph software (Gatan) or image plates (Datibis Corp). Cls1-tubulin image classification and alignment were carried out with the program SPIDER (Shaikh et al., 2008), described in detail in the Supplemental Experimental Procedures.

TIRF Microscopy Studies of Dynamic or Stable MTs with Cls1p

We used a modified version of the approach described by Brouhard et al. (2008). Tubulin dimers were labeled with succinimidyl ester or tetraflourophenyl esters of biotin, Alexa-Fluor-488 or Texas red (Invitrogen) and recycled as described by Mitchison and Kirschner (1984). MT seeds were polymerized with 2 mM GMPCPP from a 1.8 mg/ml mixture of Texas red, biotin-labeled and unlabelled tubulin dimers in a 4:2:1 ratio at 37°C for 2 hr. Glass coverslips were cleaned and silanized as described (Brouhard et al., 2008). Flow cells were constructed (Brouhard et al., 2008) and treated as described below and in the Supplemental Experimental Procedures. Fully sealed flow cells were mounted onto a Nikon microscope with a 60× Nikon TIRF objective, warmed to 35°C by a temperature collar. MTs were imaged in the evanescent wave by 488 and 568 nm laser excitation. Dual emission data were collected in 2.1 s intervals for 18.4 min (1125 s) with a side entry iXon EM CCD (Andor Sciences) with each channel projected onto split fields. Details for dynamic and stabilized MT imaging are described in Supplemental Experimental Procedures.

Image Analysis and Measurement of MT Dynamics Parameters

Image stacks were analyzed using EMBL-ImageJ software (Rasband, W.S., ImageJ, U. S. National Institutes of Health, Bethesda, Maryland, USA, http://rsb.info.nih.gov/ij/, 1997–2009). Raw image stacks were bleach corrected by normalization of total image intensity to the average intensity of the first image and scaling up the value of bleached images accordingly. Kymographs were constructed for dynamic MTs growing from each MT seed to study the transitions and rates of assembly and disassembly. MT assembly and disassembly rates were measured as slopes in kymographs of individual dynamic MTs. Frequencies of catastrophe and rescue events were measured for individual dynamic MTs formed from each seed by dividing the number of events by the duration of assembly (for catastrophe) and disassembly (for rescue). A rescue event was identified as a reversal of measurable disassembly (at least 10 pixels) to assembly. MT pauses were extremely rare and were not counted as rescue events. Further details are described in the Supplemental Experimental Procedures.

Cls1p TOG Mutants in *S. pombe*

A Stratagene Site-directed mutagenesis kit was used to introduce mutations into pREP42x nmt*-mCherry-Cls1 (1-1462) (Bratman and Chang, 2007). For induction of Cls1p expression from the *nmt1** promoter, cells were grown for 14–16 hr at 30°C in media lacking thiamine. Assays for Cls1p rescue of viability, MT stabilization and Cls1p localization are as described in Bratman and Chang (2007). Maximum intensity projections of spinning disc confocal images are shown.

SUPPLEMENTAL INFORMATION

Supplemental Information includes Supplemental Experimental Procedures, seven figures, and three tables and can be found with this article online at doi:10.1016/j.devcel.2010.07.016.

ACKNOWLEDGMENTS

We thank Anthony Hyman and Jonathon Howard and their laboratories (Max Planck Institute-CBG, Dresden) for hosting J.A.-B to gain expertise in TIRF microscopy prior to this work. We thank Scott Bratman and members of Harrison and Chang laboratories for suggestions and advice throughout this work. J.A.-B and F.C. acknowledge support from the National Institutes of Health (Pathway to Independence GMO8429 for J.A.-B) and (GM069670 for F.C.), respectively. G.J.B. acknowledges support from the Natural Sciences and Engineering Research Council of Canada (#372593-09). S.C.H is an investigator of the Howard Hughes Medical Institute.

Received: October 19, 2009
Revised: April 12, 2010
Accepted: June 30, 2010
Published: August 16, 2010

REFERENCES

Akhmanova, A., and Steinmetz, M.O. (2008). Tracking the ends: a dynamic protein network controls the fate of microtubule tips. Nat. Rev. Mol. Cell Biol. *9*, 309–322.

Al-Bassam, J., van Breugel, M., Harrison, S.C., and Hyman, A. (2006). Stu2p binds tubulin and undergoes an open-to-closed conformational change. J. Cell Biol. *172*, 1009–1022.

Al-Bassam, J., Larsen, N.A., Hyman, A.A., and Harrison, S.C. (2007). Crystal structure of a TOG domain: conserved features of XMAP215/Dis1-family TOG domains and implications for tubulin binding. Structure *15*, 355–362.

Ambrose, J.C., Shoji, T., Kotzer, A.M., Pighin, J.A., and Wasteneys, G.O. (2007). The Arabidopsis CLASP gene encodes a microtubule-associated protein involved in cell expansion and division. Plant Cell *19*, 2763–2775.

Bratman, S.V., and Chang, F. (2007). Stabilization of overlapping microtubules by fission yeast CLASP. Dev. Cell *13*, 812–827.

Bratman, S.V., and Chang, F. (2008). Mechanisms for maintaining microtubule bundles. Trends Cell Biol. *18*, 580–586.

Brouhard, G.J., Stear, J.H., Noetzel, T.L., Al-Bassam, J., Kinoshita, K., Harrison, S.C., Howard, J., and Hyman, A.A. (2008). XMAP215 is a processive microtubule polymerase. Cell *132*, 79–88.

Dimitrov, A., Quesnoit, M., Moutel, S., Cantaloube, I., Pous, C., and Perez, F. (2008). Detection of GTP-tubulin conformation in vivo reveals a role for GTP remnants in microtubule rescues. Science *322*, 1353–1356.

Drabek, K., van Ham, M., Stepanova, T., Draegestein, K., van Horssen, R., Sayas, C.L., Akhmanova, A., Ten Hagen, T., Smits, R., Fodde, R., et al. (2006). Role of CLASP2 in microtubule stabilization and the regulation of persistent motility. Curr. Biol. *16*, 2259–2264.

Du, Y., English, C.A., and Ohi, R. (2010). The kinesin-8 Kif18A dampens microtubule plus end dynamics. Curr. Biol. *20*, 374–380.

Efimov, A., Kharitonov, A., Efimova, N., Loncarek, J., Miller, P.M., Andreyeva, N., Gleeson, P., Galjart, N., Maia, A.R., McLeod, I.X., et al. (2007). Asymmetric CLASP-dependent nucleation of noncentrosomal microtubules at the trans-Golgi network. Dev. Cell *12*, 917–930.

Galjart, N., Grosveld, F., Vorobjev, I., Tsukita, S., and Akhmanova, A. (2005). CLASP1 and CLASP2 bind to EB1 and regulate microtubule plus-end dynamics at the cell cortex. J. Cell Biol. *168*, 141–153.

Gardner, M.K., and Odde, D.J. (2010). Stochastic simulation and graphic visualization of mitotic processes. Methods *51*, 251–256.

Grallert, A., Beuter, C., Craven, R.A., Bagley, S., Wilks, D., Fleig, U., and Hagan, I.M. (2006). S. pombe CLASP needs dynein, not EB1 or CLIP170, to induce microtubule instability and slows polymerization rates at cell tips in a dynein-dependent manner. Genes Dev. *20*, 2421–2436.

Gupta, M.L., Jr., Carvalho, P., Roof, D.M., and Pellman, D. (2006). Plus end-specific depolymerase activity of Kip3, a kinesin-8 protein, explains its role in positioning the yeast mitotic spindle. Nat. Cell Biol. *8*, 913–923.

Honnappa, S., Gouveia, S.M., Weisbrich, A., Damberger, F.F., Bhavesh, N.S., Jawhari, H., Grigoriev, I., van Rijssel, F.J., Buey, R.M., Lawera, A., et al. (2009). An EB1-binding motif acts as a microtubule tip localization signal. Cell *138*, 366–376.

Ichihara, K., Kitazawa, H., Iguchi, Y., Hotani, H., and Itoh, T.J. (2001). Visualization of the stop of microtubule depolymerization that occurs at the high-density region of microtubule-associated protein 2 (MAP2). J. Mol. Biol. *312*, 107–118.

Katsuki, M., Drummond, D.R., Osei, M., and Cross, R.A. (2009). Mal3 masks catastrophe events in Schizosaccharomyces pombe microtubules by inhibiting shrinkage and promoting rescue. J. Biol. Chem. *284*, 29246–29250.

Kumar, P., Lyle, K.S., Gierke, S., Matov, A., Danuser, G., and Wittmann, T. (2009). GSK3beta phosphorylation modulates CLASP-microtubule association and lamella microtubule attachment. J. Cell. Biol. *184*, 895–908.

Lansbergen, G., Grigoriev, I., Mimori-Kiyosue, Y., Ohtsuka, T., Higa, S., Kitajima, I., Demmers, J., Galjart, N., Houtsmuller, A.B., Grosveld, F., and Akhmanova, A. (2006). CLASPs attach microtubule plus ends to the cell cortex through a complex with LL5beta. Dev. Cell *11*, 21–32.

Laycock, J.E., Savoian, M.S., and Glover, D.M. (2006). Antagonistic activities of Klp10A and Orbit regulate spindle length, bipolarity and function in vivo. J. Cell Sci. *119*, 2354–2361.

Lee, H., Engel, U., Rusch, J., Scherrer, S., Sheard, K., and Van Vactor, D. (2004). The microtubule plus end tracking protein Orbit/MAST/CLASP acts downstream of the tyrosine kinase Abl in mediating axon guidance. Neuron *42*, 913–926.

Maffini, S., Maia, A.R., Manning, A.L., Maliga, Z., Pereira, A.L., Junqueira, M., Shevchenko, A., Hyman, A., Yates, J.R., III, Galjart, N., et al. (2009). Motor-independent targeting of CLASPs to kinetochores by CENP-E promotes microtubule turnover and poleward flux. Curr Biol. *19*, 1566–1572.

Maiato, H., Fairley, E.A., Rieder, C.L., Swedlow, J.R., Sunkel, C.E., and Earnshaw, W.C. (2003a). Human CLASP1 is an outer kinetochore component that regulates spindle microtubule dynamics. Cell *113*, 891–904.

Maiato, H., Rieder, C.L., Earnshaw, W.C., and Sunkel, C.E. (2003b). How do kinetochores CLASP dynamic microtubules? Cell Cycle *2*, 511–514.

Maiato, H., Khodjakov, A., and Rieder, C.L. (2005). Drosophila CLASP is required for the incorporation of microtubule subunits into fluxing kinetochore fibres. Nat. Cell Biol. *7*, 42–47.

Mimori-Kiyosue, Y., Grigoriev, I., Lansbergen, G., Sasaki, H., Matsui, C., Severin, F., Galjart, N., Grosveld, F., Vorobjev, I., Tsukita, S., and Akhmanova, A. (2005). CLASP1 and CLASP2 bind to EB1 and regulate microtubule plus-end dynamics at the cell cortex. J. Cell Biol. *168*, 141–153.

Mitchison, T., and Kirschner, M. (1984). Dynamic instability of microtubule growth. Nature *312*, 237–242.

Ookata, K., Hisanaga, S., Bulinski, J.C., Murofushi, H., Aizawa, H., Itoh, T.J., Hotani, H., Okumura, E., Tachibana, K., and Kishimoto, T. (1995). Cyclin B interaction with microtubule-associated protein 4 (MAP4) targets p34cdc2 kinase to microtubules and is a potential regulator of M-phase microtubule dynamics. J. Cell Biol. *128*, 849–862.

Pereira, A.L., Pereira, A.J., Maia, A.R., Drabek, K., Sayas, C.L., Hergert, P.J., Lince-Faria, M., Matos, I., Duque, C., Stepanova, T., et al. (2006). Mammalian CLASP1 and CLASP2 cooperate to ensure mitotic fidelity by regulating spindle and kinetochore function. Mol. Biol. Cell *17*, 4526–4542.

Pryer, N.K., Walker, R.A., Skeen, V.P., Bourns, B.D., Soboeiro, M.F., and Salmon, E.D. (1992). Brain microtubule-associated proteins modulate microtubule dynamic instability in vitro. Real-time observations using video microscopy. J. Cell Sci. *103*, 965–976.

Shaikh, T.R., Gao, H., Baxter, W.T., Asturias, F.J., Boisset, N., Leith, A., and Frank, J. (2008). SPIDER image processing for single-particle reconstruction of biological macromolecules from electron micrographs. Nat. Protoc. *3*, 1941–1974.

Slep, K.C. (2009). The role of TOG domains in microtubule plus end dynamics. Biochem. Soc. Trans. *37*, 1002–1006.

Slep, K.C., and Vale, R.D. (2007). Structural basis of microtubule plus end tracking by XMAP215, CLIP-170, and EB1. Mol. Cell *27*, 976–991.

Sousa, A., Reis, R., Sampaio, P., and Sunkel, C.E. (2007). The Drosophila CLASP homologue, Mast/Orbit regulates the dynamic behaviour of interphase microtubules by promoting the pause state. Cell Motil. Cytoskeleton *64*, 605–620.

Walker, R.A., O'Brien, E.T., Pryer, N.K., Soboeiro, M.F., Voter, W.A., Erickson, H.P., and Salmon, E.D. (1988). Dynamic instability of individual microtubules analyzed by video light microscopy: rate constants and transition frequencies. J. Cell Biol. *107*, 1437–1448.

Wittmann, T., and Waterman-Storer, C.M. (2005). Spatial regulation of CLASP affinity for microtubules by Rac1 and GSK3beta in migrating epithelial cells. J. Cell Biol. *169*, 929–939.

Yin, H., You, L., Pasqualone, D., Kopski, K.M., and Huffaker, T.C. (2002). Stu1p is physically associated with beta-tubulin and is required for structural integrity of the mitotic spindle. Mol. Biol. Cell *13*, 1881–1892.